

Calibration of the ART-XC mirror modules at MSFC

R. Krivonos¹ · A. Tkachenko¹ ·
R. Burenin¹ · E. Filippova¹ · I. Lapshov¹ ·
I. Mereminskiy¹ · S. Molkov¹ · M. Pavlinsky¹ ·
S. Sazonov^{1,2} · M. Gubarev³ ·
J. Kolodziejczak³ · S.L. O'Dell³ · D. Swartz³ ·
Vyacheslav E. Zavlin³ · B.D. Ramsey³

Dedicated to Mikhail Gubarev

Received: 23 May 2017 / Accepted: 28 Jul 2017

Abstract The Astronomical Röntgen Telescope X-ray Concentrator (ART-XC) is a hard X-ray telescope with energy response up to 30 keV, to be launched on board the Spectrum Röntgen Gamma (SRG) spacecraft in 2018. ART-XC consists of seven identical co-aligned mirror modules. Each mirror assembly is coupled with a CdTe double-sided strip (DSS) focal-plane detector. Eight X-ray mirror modules (seven flight and one spare units) for ART-XC were developed and fabricated at the Marshall Space Flight Center (MSFC), NASA, USA. We present results of testing procedures performed with an X-ray beam facility at MSFC to calibrate the point spread function (PSF) of the mirror modules. The shape of the PSF was measured with a high-resolution CCD camera installed in the focal plane with defocusing of 7 mm, as required by the ART-XC design. For each module, we performed a parametrization of the PSF at various angular distances Θ . We used a King function to approximate the radial profile of the near on-axis PSF ($\Theta < 9$ arcmin) and an ellipse fitting procedure to describe the morphology of the far off-axis angular response ($9 < \Theta < 24$ arcmin). We found a good agreement between the seven ART-XC flight mirror modules at the level of 10%. The on-axis angular resolution of the ART-XC optics varies between 27 and 33 arcsec (half-power diameter), except for the spare module.

Keywords X-ray astrophysics · Instrumentation:X-ray optics

R. Krivonos

¹Space Research Institute of the Russian Academy of Sciences,
Profsoyuznaya Str. 84/32, 117997 Moscow, Russia;
E-mail: krivonos@iki.rssi.ru

²Moscow Institute of Physics and Technology, Institutsky per. 9, 141700 Dolgoprudny, Russia

³NASA/Marshall Space Flight Center, Huntsville, Alabama 35812, USA

1 Introduction

The Spectrum-Röntgen-Gamma (SRG) mission is a Russian-German X-ray astrophysical observatory that carries two co-aligned X-ray telescope systems, the German-led extended ROentgen Survey with an Imaging Telescope Array (eROSITA, [1]) and the Russian-led Astronomical Röntgen Telescope X-ray Concentrator (ART-XC, [2]). Both telescope systems consist of 7 independent mirror modules and focal plane detectors, operating in 0.2 – 10 keV (eROSITA) and 5 – 30 keV (ART-XC). SRG is planned to be launched in 2018 using a Proton-M rocket with a Blok DM-2 upper stage from the Baikonur Cosmodrome into an orbit around L2.

eROSITA, the primary instrument of the SRG mission, will perform a deep survey of the entire sky in the soft (0.5-2 keV) and medium (2-10 keV) X-ray bands, providing the most sensitive X-ray survey ever made. ART-XC will extend the energy coverage of SRG up to ~ 30 keV, contributing to the eROSITA survey by gathering complementary information about celestial hard X-ray sources. ART-XC will perform an all-sky hard X-ray survey almost unaffected by the obscuration bias typical for softer X-ray surveys, and provide a census of intrinsically strongly absorbed objects such as Compton thick active galactic nuclei (AGNs) and heavily obscured Galactic X-ray binary systems. Science goals of the ART-XC telescope include studies of massive nearby galaxy clusters; timing and broad band spectroscopy (up to 30 keV) of Galactic objects (including X-ray binaries, anomalous pulsars and supernova remnants); search for cyclotron line features in X-ray pulsar spectra; exploration of non-thermal components in the Galaxy diffuse emission; etc.

Accurate knowledge of an X-ray telescope's response to a point X-ray source is essential for its effective use. Here, we report the results of our calibrations of the angular response of the ART-XC mirror modules using high-resolution CCD images of the telescope's point spread function (PSF) provided by MSFC. We have performed a parametrization of the PSF at different off-axis distances, which will be included into the calibration data base (CALDB) of the ART-XC telescope, part of the data reduction software and high-level scientific analysis.

2 ART-XC Mirror Modules

The X-ray mirror modules for ART-XC were designed and fabricated at MSFC. Four flight modules were produced under an International Reimbursable Agreement between NASA and the Space Research Institute (IKI) in Moscow, Russia, and three flight modules and one spare unit were fabricated under a Cooperative Agreement between NASA and IKI. The details of the mirror design and development can be found in [3,4,5]. Each module consists of 28 concentrically nested (two-reflection) grazing-incidence mirrors made of an electroformed nickel-cobalt alloy and mounted on a single spider through combs glued onto the spider legs. The spider of each mirror module is fixed to the support plate on the top of the optical bench. The shells vary in thickness from 250 μm (inner) to 350 μm (outer) and range in diameter from about 50 mm to 150 mm. The total length of the primary and secondary mirror surfaces is 580 mm. The ART-XC shell mirrors are coated with iridium (Ir) to enhance their

high-energy reflectivity up to 30 keV [6, 7]. The nominal focal length of the ART-XC mirror modules is 2700 mm. The actual values for the seven flight modules are in good mutual agreement (see below).

The ART-XC field of view (FOV) is 36 arcmin in diameter, which is mainly determined by the working area of the CdTe focal plane detectors (28.56×28.56 mm, [2]). According to a raytrace simulation model of the ART-XC mirror optics, the effective-area drop (vignetting) at the FOV edge is about 20% at 8 keV (Tkachenko et al., in preparation).

A number of angular resolution measurements were performed to determine the optimal angular resolution across the FOV. It was found that defocusing a module by intra-focal 7 mm provides more uniform angular resolution across the FOV compared to the resolution at the nominal focal distance [5]. In the following, we adopt each ART-XC module being defocused by 7 mm as a default ART-XC design, unless otherwise stated.

The flight-grade mirror modules numbered as ARTM1-5,7,8 were transported to Sarov (Russia) in 2016 for the final assembly with the telescope baffle system and focal plane detectors. One spare module, ARTM6, was delivered to IKI for testing at a 60-meter X-ray beam facility. The flight model of the ART-XC telescope with all seven mirror modules, after acceptance tests, was transported to the Lavochkin Association (Khimki, Russia) in December 2016 for integration with the SRG spacecraft.

3 ART-XC mirror tests

The ART-XC mirror modules were extensively tested with a 104-meter X-ray beam facility at MSFC [5]. The distance from the radiation source to the principal plane of the mirror module, i.e., the object distance, was 103.3 m. In the thin lens approximation, the nominal focal length 2700 mm results in an image distance of 2772 mm. To measure the spatial shape of the PSF at the best available quality, a high-resolution CCD sensor ANDOR iKon-L 936 with a pixel size of $13.5 \times 13.5 \mu\text{m}$ was installed 2765 mm from the mirror module's principal plane, resulting in a defocus of 7 mm intra-focal.

The radiation source was a copper anode of the X-ray tube with applied 15 kilovolt voltage. The spectrum of the X-ray source is thus dominated by copper (Cu) $K\alpha$ and $K\beta$ lines, at 8.04 and 8.9 keV, respectively. Thus, the angular response of the ART-XC mirrors was calibrated at MSFC using an almost monochromatic X-ray beam at energy ~ 8 keV. Note that the testing procedures were done without the baffle of the telescope, which was installed later, after assembling the telescope in Sarov.

Each ART-XC mirror module was tilted with respect to the X-ray beam in order to obtain PSF images at off-axis angles $\Theta = 0, 1, 3, 5, 7, 9, 12, 15$ and 18 arcmin and azimuthal angles $\Phi = 0^\circ, 45^\circ, 90^\circ$ and 135° , as illustrated in Fig. 1. As seen from a sample of original ARTM1 PSF images (Fig. 2), the shape of the angular response remains nearly regular within 9 arcmin from the optical axis.

MSFC has also carried out calibrations of ARTM7 angular response at extreme off-axis distances $\Theta = 20, 22$ and 24 arcmin (Fig. 3), to simulate a halo of ghost rays

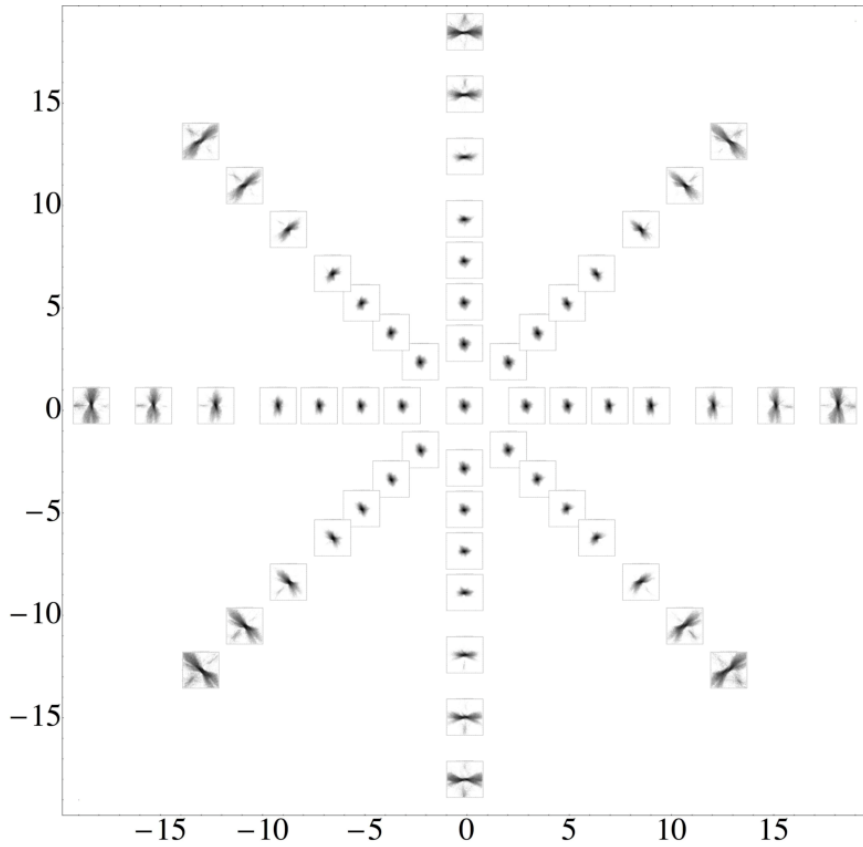


Fig. 1 The mosaic illustrates the PSF of ARTM1 in scans at different azimuthal angles $\Phi = 0^\circ, 45^\circ, 90^\circ$ and 135° , and angular distances $\Theta = 0, 3, 5, 7, 9, 12, 15$ and 18 arcmin. PSF images at 1 arcmin are not shown for clarity.

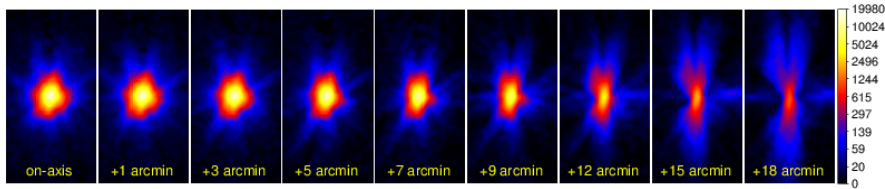


Fig. 2 A sample of nine original ARTM1 PSF images at different angular distances $\Theta = 0 - 18$ arcmin from the mirror's optical axis. One image pixel corresponds to $2 \times 13.5 \mu m$ or ~ 2 arcsec, calculated for a detector distance of 2765 mm (7 -mm intra-focal defocus). The size of each image box is $\sim 2 \times 4$ mm or $\sim 150 \times 300$ arcsec. Hereafter, the PSF images are background subtracted and smoothed with a 3 pixel width tophat filter in DS9 (SAOImage astronomical imaging and data visualization application) for better view. The logarithmic color map ranges from 0 to the peak value of the on-axis PSF.

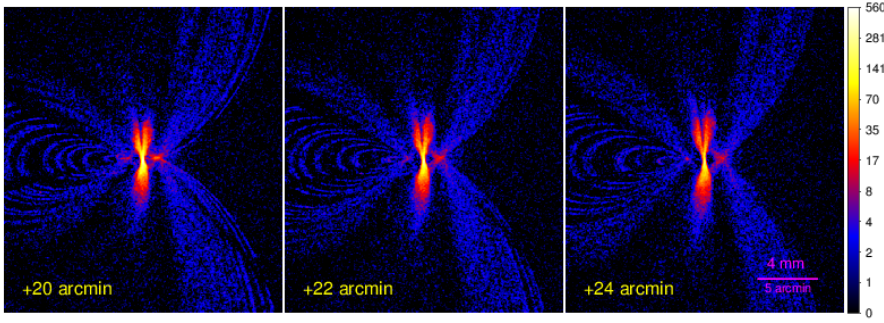


Fig. 3 A sample of three original ARTM7 PSF images at extreme angular distances $\Theta = 20, 22$ and 24 arcmin. The size of the images is $\sim 18 \times 20$ mm or $\sim 23 \times 25$ arcmin. The logarithmic color map ranges from 0 to the peak value of the PSF at $\Theta = 20$ arcmin.

(single-reflection photons), from a bright source located nearly outside the FOV of the ART-XC telescope.

4 PSF image reduction

One of the main goals of this work is to build a simple analytical representation of the PSF for each ART-XC mirror module at different off-axis distances. The CCD images of the ART-XC PSF provided by MSFC (Fig. 1) contain relevant information about the construction of the mirror modules, e.g. the shadow of the spider structure visible at different azimuthal directions, misalignment of the mirror shells, etc. For instance, Fig. 2 shows that even the on-axis PSF of ARTM1 is characterized by a non-uniform and slightly asymmetric shape, which does not change with azimuthal rotation. We keep the original PSF images in the ART-XC calibration data base for possible future use if a detailed knowledge of the ART-XC PSF is needed. Studying the radial profiles of the on-axis PSF for the different mirror modules, we found that the systematic deviation between the modules can reach 20 – 30%. The angular size of the ART-XC detector element of ~ 45 arcsec is a factor of 1.5 larger than the ~ 30 arcsec half-power diameter (HPD, corresponding to half of the focused X-rays) of the optics [2], which allows us to suppress detailed structures of the PSF for simplicity, by averaging them azimuthally at a given off-axis angle.

To make an average PSF for each mirror module, we first determined the centroid position of each raw PSF within the HPD around the PSF maximum. The relative systematic offset between the centroid positions did not exceed $135 \mu\text{m}$ (or ~ 10 arcsec) across the FOV. Each PSF image was shifted to the centroid position and rotated at the corresponding azimuthal angle, to align all PSF images in one direction, with the optical axis position to the north. In this way, the images were stacked together to produce an averaged PSF image at a given off-axis distance. Note that we ascribed the stacked PSF images at angular distances 20, 22 and 24 arcmin measured for ARTM7 only (Fig. 3) to all mirror modules, in order to have uniform off-axis coverage in the ART-XC calibration data base. Figure 4 shows average PSF images for the ARTM1 mirror module.

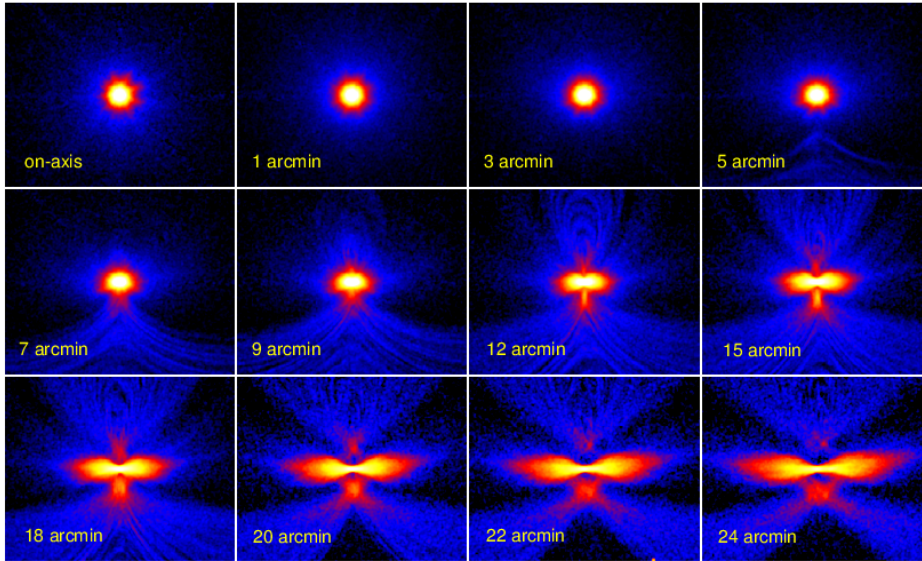


Fig. 4 Average PSF images for the ARTM1 mirror module at different off-axis distances Θ . The size of each image is $\sim 10 \times 8$ mm or $\sim 13 \times 10$ arcmin. Note that PSF images at $\Theta = 20, 22$ and 24 arcmin were measured for ARTM7 only and were ascribed to all mirror modules.

5 Parametrization of the ART-XC Point Spread Function

In this section, we describe the average PSF shape of each ART-XC mirror module at different off-axis distances. We divide PSF images into two groups. The first, “near on-axis”, group comprises all off-axis distances within 9 arcmin from the optical axis. This group is characterized by a virtually regular shape of the PSF, which can be represented analytically. The second, “far off-axis”, group includes all PSFs at angular distances larger than 9 arcmin, where off-axis aberrations are severe. In this case, we apply a simple contoured parameterization of the PSF, which is nevertheless useful for many analysis purposes.

5.1 Near on-axis PSF

Figure 5 shows the radial profile of the on-axis PSF for the ARTM1 mirror module. The PSF shape of the Wolter-I optics is characterized by a narrow core and wide wings at offsets larger than 100 arcsec (see e.g. the *NuSTAR* optics’ calibration [8]). Both components can be approximated in terms of King’s function [9]:

$$K(r, \sigma, \gamma) = \left(1 + \frac{r^2}{\sigma^2}\right)^{-\gamma} \quad (1)$$

The parameter σ is the characteristic size of the core, γ determines the weight of the tails, and r is the angular offset in arcsec. We represent the 2D profile of the ART-XC

Table 1 Best-fitting model parameters of the decomposition of the ART-XC PSF with the use of linear combination of two King functions.

Module	Off-axis distance Θ (arcmin)					
	0	1	3	5	7	9
	$N_{\text{core}} (\times 10^{-3} \text{ arcsec}^2)$					
ARTM1	1.81 ± 0.14	1.85 ± 0.14	1.98 ± 0.15	1.97 ± 0.15	1.76 ± 0.14	1.25 ± 0.10
ARTM2	1.47 ± 0.11	1.53 ± 0.12	1.63 ± 0.12	1.58 ± 0.12	1.40 ± 0.11	1.02 ± 0.08
ARTM3	1.55 ± 0.12	1.59 ± 0.12	1.70 ± 0.13	1.76 ± 0.14	1.64 ± 0.13	1.29 ± 0.10
ARTM4	1.24 ± 0.09	1.26 ± 0.10	1.35 ± 0.10	1.38 ± 0.11	1.29 ± 0.10	1.06 ± 0.09
ARTM5	1.59 ± 0.12	1.62 ± 0.13	1.65 ± 0.13	1.63 ± 0.13	1.41 ± 0.11	0.94 ± 0.07
ARTM6	0.82 ± 0.06	0.85 ± 0.06	0.87 ± 0.06	0.76 ± 0.05	0.74 ± 0.05	0.63 ± 0.05
ARTM7	1.34 ± 0.10	1.39 ± 0.10	1.49 ± 0.11	1.47 ± 0.11	1.30 ± 0.10	1.01 ± 0.08
ARTM8	1.18 ± 0.09	1.24 ± 0.09	1.33 ± 0.10	1.31 ± 0.10	1.16 ± 0.09	0.92 ± 0.07
	σ_{core} (arcsec)					
ARTM1	12.8 ± 0.3	12.7 ± 0.3	12.3 ± 0.3	12.0 ± 0.3	12.5 ± 0.3	14.5 ± 0.4
ARTM2	14.3 ± 0.4	14.0 ± 0.4	13.6 ± 0.3	13.5 ± 0.3	14.0 ± 0.4	16.0 ± 0.5
ARTM3	13.9 ± 0.3	13.7 ± 0.3	13.3 ± 0.3	12.7 ± 0.3	12.8 ± 0.3	14.1 ± 0.4
ARTM4	15.5 ± 0.4	15.4 ± 0.4	14.9 ± 0.4	14.5 ± 0.4	14.6 ± 0.4	15.6 ± 0.5
ARTM5	13.6 ± 0.4	13.4 ± 0.4	13.3 ± 0.3	13.2 ± 0.4	13.9 ± 0.4	16.3 ± 0.5
ARTM6	18.7 ± 0.5	18.5 ± 0.4	18.1 ± 0.4	18.1 ± 0.4	18.6 ± 0.5	19.6 ± 0.6
ARTM7	14.9 ± 0.4	14.6 ± 0.4	14.2 ± 0.4	14.0 ± 0.4	14.5 ± 0.4	16.0 ± 0.5
ARTM8	15.9 ± 0.4	15.5 ± 0.4	15.0 ± 0.4	14.8 ± 0.4	15.2 ± 0.4	16.7 ± 0.5
	σ_{wing} (arcsec)					
ARTM1	237 ± 27	252 ± 36	263 ± 42	417 ± 90	325 ± 46	272 ± 35
ARTM2	216 ± 35	215 ± 29	218 ± 33	391 ± 80	319 ± 46	265 ± 32
ARTM3	268 ± 48	263 ± 38	274 ± 45	383 ± 72	338 ± 48	269 ± 31
ARTM4	193 ± 30	196 ± 25	179 ± 24	242 ± 36	239 ± 28	208 ± 22
ARTM5	200 ± 27	198 ± 22	232 ± 30	235 ± 29	232 ± 28	261 ± 32
ARTM6	405 ± 112	394 ± 85	426 ± 103	659 ± 239	405 ± 74	313 ± 44
ARTM7	239 ± 49	238 ± 38	242 ± 43	332 ± 66	276 ± 42	212 ± 27
ARTM8	250 ± 49	245 ± 37	251 ± 41	355 ± 67	299 ± 42	243 ± 29
	$f_{\text{wing}} (\times 10^{-4})$					
ARTM1	1.9 ± 0.4	1.6 ± 0.4	1.2 ± 0.3	1.0 ± 0.2	2.5 ± 0.5	6.1 ± 1.1
ARTM2	2.7 ± 0.9	2.6 ± 0.7	1.9 ± 0.6	1.3 ± 0.3	3.2 ± 0.6	8.1 ± 1.5
ARTM3	1.7 ± 0.5	1.7 ± 0.4	1.4 ± 0.4	1.3 ± 0.3	2.6 ± 0.5	6.6 ± 1.1
ARTM4	4.5 ± 1.4	4.4 ± 1.2	4.5 ± 1.3	3.3 ± 0.8	6.1 ± 1.2	13.0 ± 2.4
ARTM5	4.2 ± 1.1	4.1 ± 0.9	3.2 ± 0.7	3.9 ± 0.8	6.1 ± 1.2	10.6 ± 1.9
ARTM6	2.1 ± 0.7	2.2 ± 0.6	2.0 ± 0.6	2.1 ± 0.5	5.4 ± 1.1	12.3 ± 2.3
ARTM7	2.8 ± 1.0	2.6 ± 0.8	2.2 ± 0.7	2.0 ± 0.5	4.7 ± 1.0	13.1 ± 2.7
ARTM8	2.6 ± 0.9	2.7 ± 0.8	2.2 ± 0.7	2.0 ± 0.5	4.6 ± 0.9	11.5 ± 2.2

near on-axis PSF as a linear combination of two King functions:

$$PSF(r) = N_{\text{core}} \times [f_{\text{core}} K(r, \sigma_{\text{core}}, \gamma_{\text{core}}) + f_{\text{wing}} K(r, \sigma_{\text{wing}}, \gamma_{\text{wing}})], \quad (2)$$

where N_{core} is an arbitrary overall normalization factor and $f_{\text{core}} + f_{\text{wing}} = 1$. Due to degeneracy between the σ and γ parameters, we fixed the latter at $\gamma = 2$ both for the core and the wing. This also makes possible a direct comparison of the model parameters amongst the mirror modules.

The stacked PSF images contain a large number of counts per pixel ($> 10^4$ in the core), which translates into small statistical errors in the radial profile. As the fitting

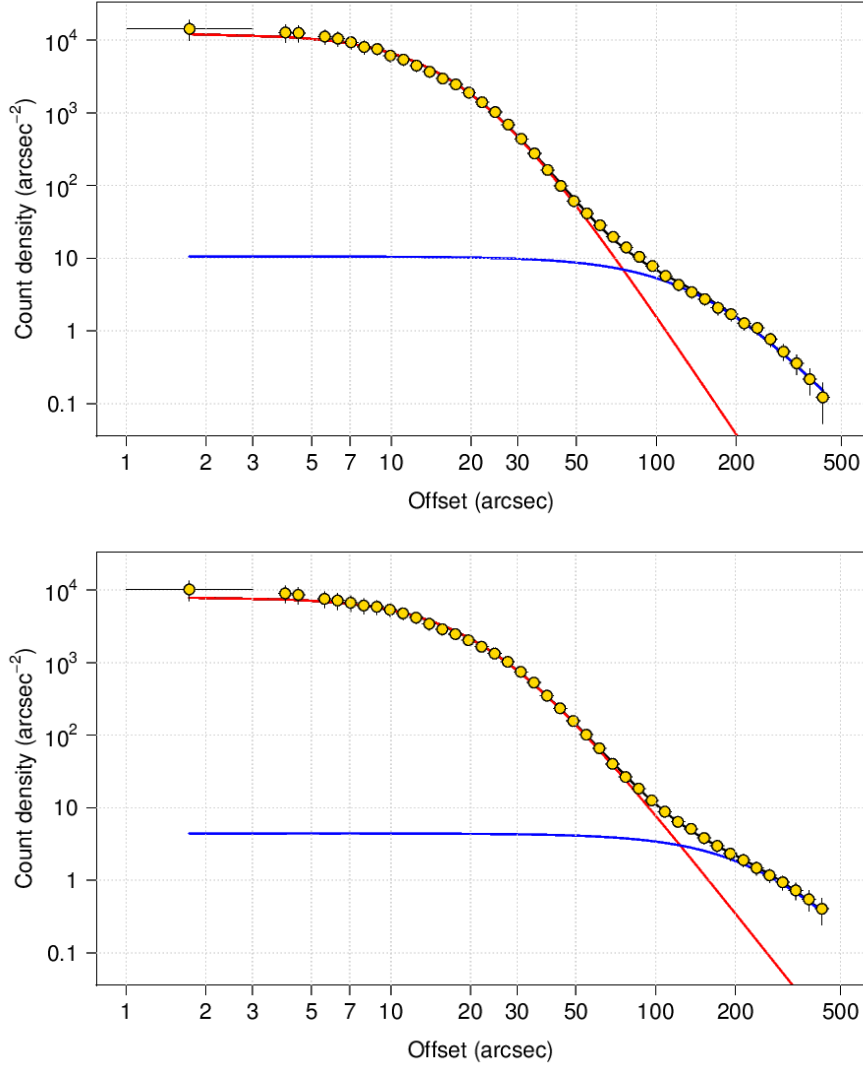


Fig. 5 Radial profile of the on-axis PSF measured with the flight ARTM1 (top panel) and spare ARTM6 (bottom panel) mirror modules in 7 mm defocused regime. The King profiles for the PSF core and wing are shown with solid red and blue lines, respectively.

procedure weights the data according to the assigned errors, the data points at $r > 100$ arcsec with larger errors are weighted less in the fit, leading to a loss of sensitivity to the non-central parts of the PSF. To overcome this difficulty, and to take intrinsic PSF distortions (Sect. 4) into account, we added a fractional systematic error of 30% to the PSF radial profile. As can be seen from Fig. 5, the King-function approximation provides a good fit to the radial profile of the ART-XC PSF. The best-fitting values of the free parameters N_{core} , σ_{core} , f_{wing} and σ_{wing} for all ART-XC mirror modules are

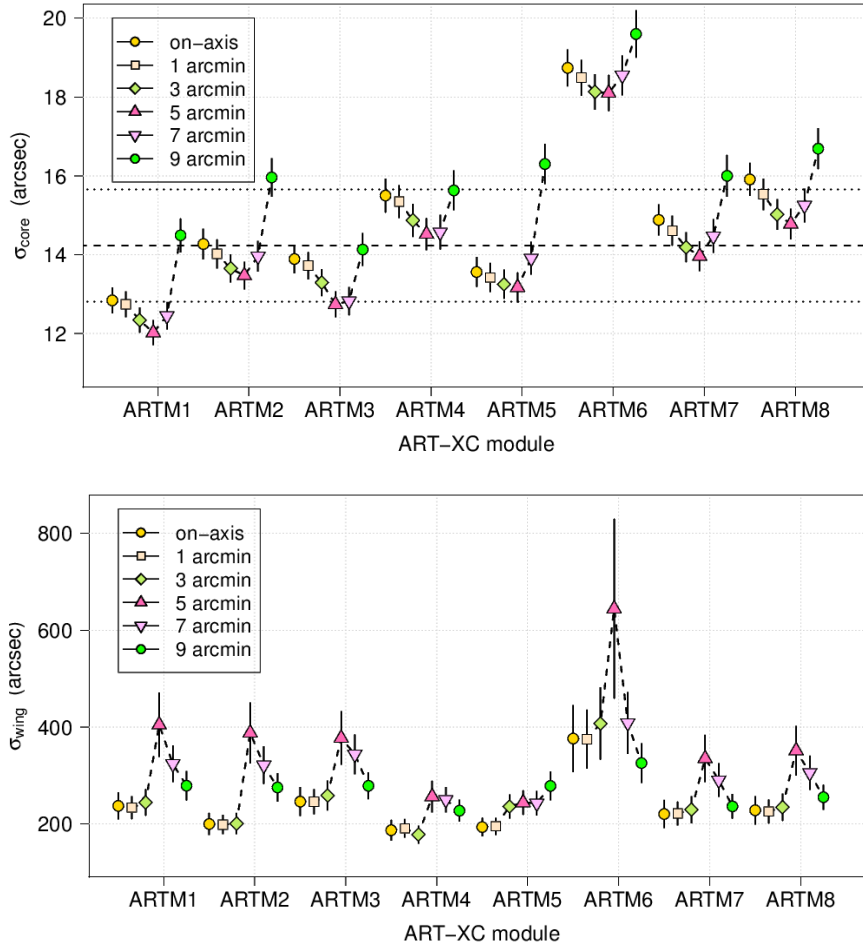


Fig. 6 Comparison of the PSF core (top panel) and wing (bottom panel) characteristic sizes (σ_{core} and σ_{wing} parameters in Eq. 1-2, respectively) between the ART-XC mirror modules for different off-axis distances within 9 arcmin. The dashed line in the top panel shows the average value of σ_{core} (14.2 arcsec), derived for the on-axis PSFs and all ART-XC mirror modules except the spare ARTM6. Dotted lines denote the 10% interval with respect to the average value.

listed in Table 1. Note that we have renormalized N_{core} so that

$$\int_{\text{FOV}} \text{PSF}(r) d\Omega = \int_0^{2\pi} \int_0^{\infty} \text{PSF}(r) r dr d\phi = 1. \quad (3)$$

Figure 6 compares the best fitting σ_{core} parameter between the mirror modules for different off-axis distances within 9 arcmin. The PSF core widths for all ART-XC flight modules are consistent with an average σ_{core} of 14.2 arcsec to within 10%, except for ARTM6, which, as mentioned above, was selected as a spare unit and will be reserved for future ground tests. As seen from Fig. 6, σ_{core} demonstrates a

Table 2 Total HPD, W90 and the contribution of the wing component to the total EEF at $R = \infty$, at a defocus of 7 mm (intra-focal).

Module	Off-axis distance Θ (arcmin)					
	0	1	3	5	7	9
	HPD (arcsec)					
ARTM1	27.4	27.0	26.3	27.0	29.7	36.6
ARTM2	30.6	29.7	28.5	30.2	33.2	40.9
ARTM3	29.7	29.3	28.1	28.5	31.0	36.6
ARTM4	33.2	33.2	31.9	32.3	35.1	40.3
ARTM5	29.7	29.3	29.3	30.2	33.7	43.8
ARTM6	41.5	40.9	40.3	47.6	48.3	54.7
ARTM7	31.9	31.4	30.2	31.4	35.1	41.5
ARTM8	33.7	33.2	31.9	33.2	36.6	43.2
	W90 (arcsec)					
ARTM1	120.2	116.1	108.3	286.3	449.6	516.5
ARTM2	128.8	124.5	112.1	240.7	449.6	534.8
ARTM3	128.8	124.5	116.1	258.0	534.8	573.2
ARTM4	143.0	143.0	133.4	182.3	365.0	465.4
ARTM5	158.7	153.3	170.1	249.2	365.0	636.1
ARTM6	249.2	249.2	286.3	1413.4	869.4	811.1
ARTM7	143.0	138.1	128.8	258.0	449.6	481.9
ARTM8	143.0	143.0	133.4	276.5	465.4	534.8
	Wings fraction in EEF at $R = \infty$ (%)					
ARTM1	6.0	5.9	5.3	10.5	14.4	17.8
ARTM2	6.0	5.8	4.8	9.6	14.2	18.5
ARTM3	6.1	6.0	5.6	10.1	15.4	19.6
ARTM4	6.6	6.7	6.2	8.6	14.3	19.2
ARTM5	8.4	8.3	8.8	11.2	14.8	21.8
ARTM6	8.8	8.9	9.5	21.2	20.5	24.3
ARTM7	6.7	6.6	6.1	10.2	15.0	19.2
ARTM8	6.1	6.3	5.9	10.3	15.2	19.8

decrease below $\Theta = 3$ arcmin, followed by a rise at larger off-axis angles. Since the fitting procedure optimizes a linear combination of two King profiles, σ_{wing} shows the opposite behavior.

Using the obtained analytic form (Eq. 1-2) of the PSF, we then calculated the enclosed energy fraction (EEF) as a function of angular offset r and the corresponding HPD for each PSF. The typical EEF for the near on-axis ART-XC PSF is shown in Fig. 7 (ARTM1 and ARTM6, on-axis). Half of the total EEF for the King function (Eq. 1) with $\gamma = 2$ is reached at an angular offset $r = \sigma$, so that HPD corresponds to $2 \times \sigma$. For the two-component PSF, the presence of broad wings increases the total HPD by 6% or more, e.g. for the ARTM1 EEF shown in Fig. 7, $\text{HPD}_{\text{core}} = 2 \times \sigma_{\text{core}} = 25.6 \pm 0.4$ arcsec, and $\text{HPD}_{\text{total}} = 27.4$ arcsec. Table 2 lists the total HPD and W90 (enclosed 90% energy, diameter) values for each near on-axis ART-XC PSF, and the contribution of the wing component to the total EEF calculated at $r = \infty$.

Finally, we provide a parametrization of the PSF measured in the nominal focus of the ARTM1 mirror module with on-axis setting, and tilted at off-axis distances 3 and 7 arcmin (Table 3). The total HPD (core+wing) of the on-axis PSF is 24.2 arcsec, which is $\sim 12\%$ less than the on-axis HPD in the defocused mode (27.4 arcsec). The difference in HPD for $\Theta = 7$ arcmin and on-axis PSF is 30%, while in the defocused

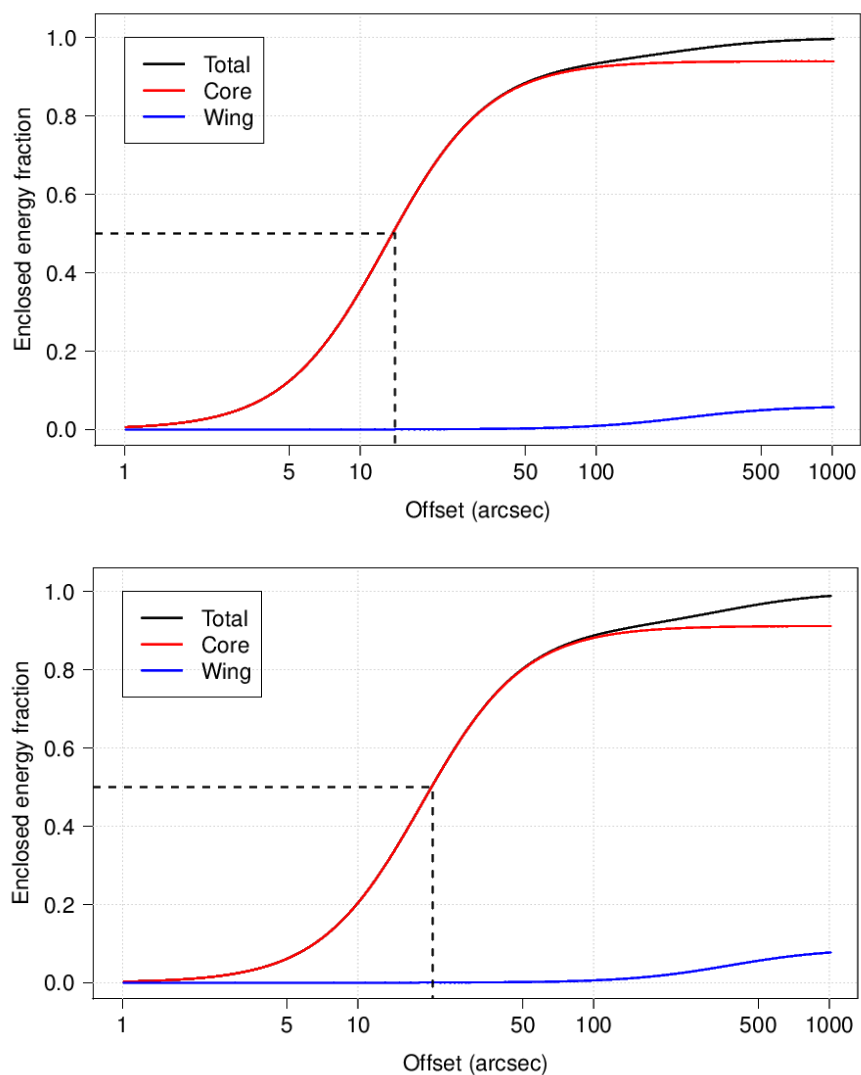


Fig. 7 Enclosed energy fraction of the on-axis PSF (top: ARTM1, bottom: ARTM6) at 7-mm defocus, derived from the analytic form Eq. 1-2 for the PSF core (red) and wing (blue) components, and total (black). Half of the total EEF, corresponding to the HPD value, is shown by the dashed line.

mode it is not more than 10%, which confirms the advantage of the ART-XC defocused mode selected for uniform angular resolution across the FOV (see Fig. 6 in [5]).

Table 3 Parametrization of the ART-XC PSF with the use of linear combination of two King functions (Eq. 2), obtained in the nominal focus mode. The information is available for ARTM1 only.

Parameter	Off-axis distance Θ (arcmin)		
	0	3	7
$N_{\text{core}} (\times 10^{-3} \text{ arcsec}^2)$	2.42 ± 0.20	2.43 ± 0.20	1.61 ± 0.13
$\sigma_{\text{core}} (\text{arcsec})$	11.1 ± 0.3	11.1 ± 0.3	13.0 ± 0.3
$\sigma_{\text{wing}} (\text{arcsec})$	187 ± 16	201 ± 16	395 ± 53
$f_{\text{wing}} (\times 10^{-4})$	2.7 ± 0.5	2.0 ± 0.4	1.9 ± 0.3
HPD (arcsec)	24.2	23.8	31.0
W90 (arcsec)	115.5	103.4	567.5
Wings EEF fraction (%)	7.3	6.2	14.8

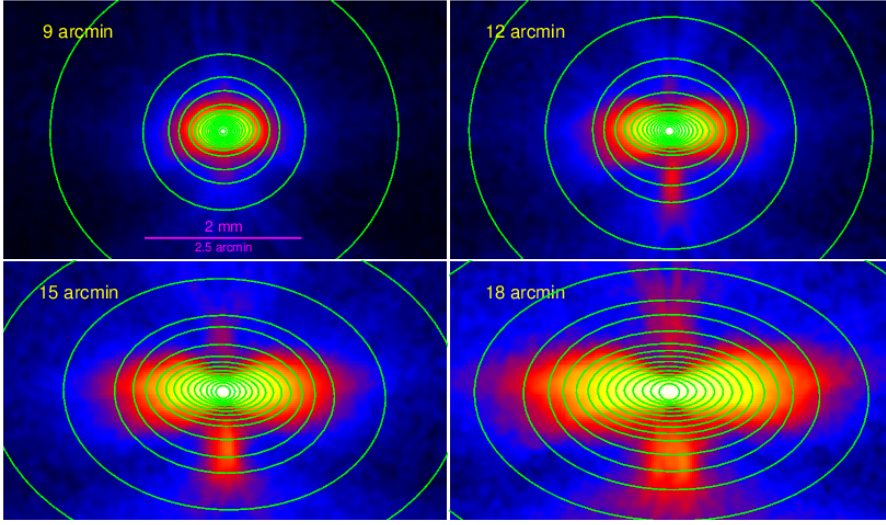


Fig. 8 Average ARTM1 PSF images at large off-axis angles of 9, 12, 15 and 18 arcmin. Green ellipses demonstrate the action of the fitting technique, revealing the elongated morphology of the PSF at different offset distances.

5.2 Far off-axis PSF

Due to the complex shape of the PSF at large angular distances (> 9 arcmin), it cannot be easily decomposed into model components. However, a zero-order description of the PSF can be made in terms of an encircled energy function, characterizing the PSF with the fractional energy measured within a circular aperture as a function of radius. We used this approach in the previous section to compare the ART-XC modules with each other for circular-symmetric PSFs at off-axis distances less than 9 arcmin.

Similar to other X-ray focusing telescopes, the PSF of the ART-XC optics becomes elongated with increasing off-axis angle, so that elliptical apertures are more suitable for representing the underlying PSF. We applied a simple technique that was developed by [10] for fitting the ray-traced Chandra PSF at large off-axis angles. The authors introduced an enclosed count fraction (ECF) within elliptical regions, analo-

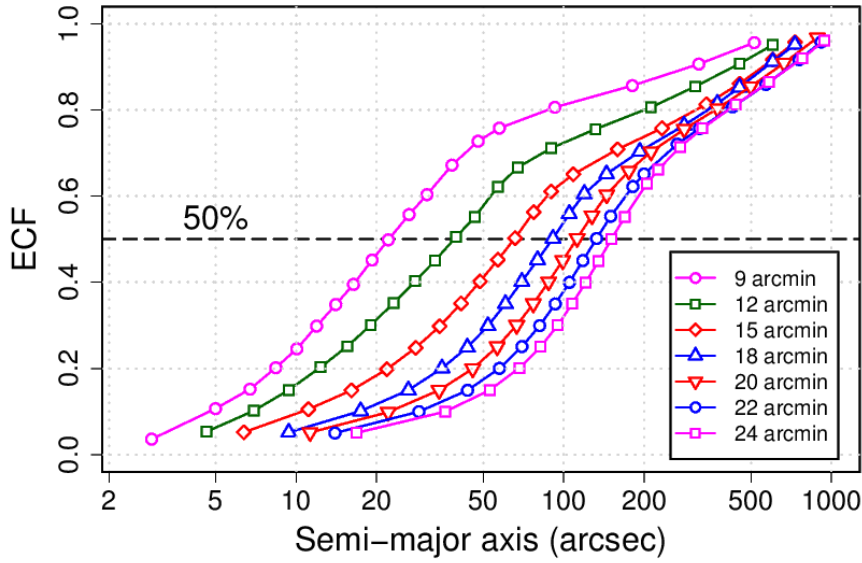


Fig. 9 ECF within a given ellipse as a function of semi-major axis for the ARTM1 PSF at different off-axis distances $\Theta = 9 - 24$ arcmin.

gous to the encircled energy function. In our study, the difference between ECF and EEF is that the former defines 100% counts at a large offset $r \sim 15$ arcmin, the size of the focal plane CCD, whereas the latter calculates the EEF at $r = \infty$. The ECF and the properties of the elliptical regions provide a parameterization of the PSF at large off-axis angles, which can be used in real observations.

Figure 8 shows an example of the ellipse fitting technique applied to the ARTM1 PSF at off-axis distances of 9, 12, 15 and 18 arcmin. The derived ellipses provide a regular and smooth approximation of the PSF morphology. Note that the ellipse fitting procedure does not provide ellipse construction at large radii, where the weight of the data is low (see the method's implementation in [10]). We thus extended the largest available ellipse by a linear scaling factor to cover the full range of offsets. We constructed ellipses to compose the ECF that are multiples of 5% within the range 5-95%. Tables 4 and 5 list ellipse parameters for ARTM1-5,7,8 at $\Theta = 9, 12, 15$ and 18 arcmin, and ARTM7 at $\Theta = 20, 22,$ and 24 arcmin, respectively. Figure 9 shows a typical ECF as a function of ellipse semi-major axis derived for ARTM1.

The ellipse fitting algorithm reveals different ellipticity of the PSF at different off-set distances r from the center. The shape of the PSF near the peak, at $r < 10$ arcsec, is almost circular, which implies that the PSF maximum is one-peaked and smooth. At medium offsets $10 < r < 70$ arcsec, PSF is strongly elongated, and the overall ellipticity increases with the off-axis angle. At large offsets $r > 100$ arcsec, the ellipticity decreases, so that the PSF becomes almost circular. Figure 10 illustrates the ellipticity as a function of semi-major axis for the constructed set of ellipses for ARTM1.

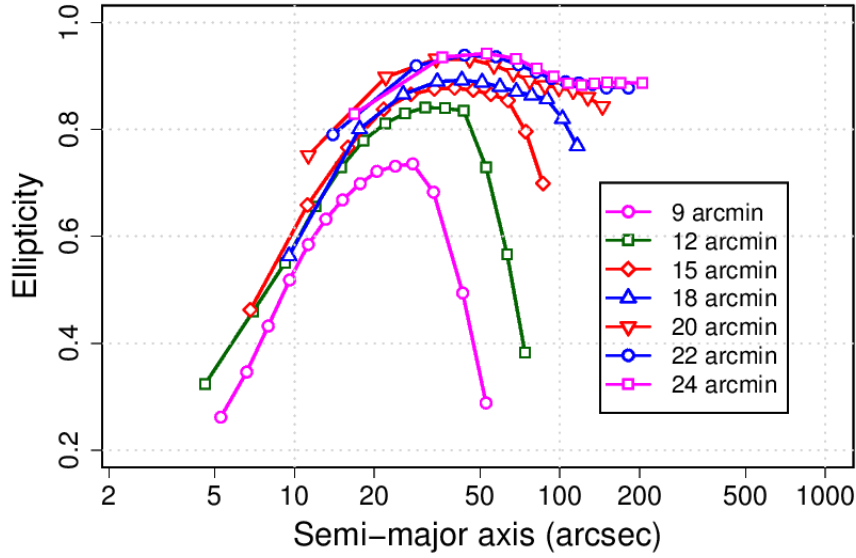


Fig. 10 Ellipticity as a function of semi-major axis for the ellipses used to describe the elongation of the ARTM1 PSF at different off-axis distances $\theta = 9 - 24$ arcmin.

Table 4 Parameterization of the ART-XC PSF in a form of ellipse semi-major (a) and minor (b) axes with a corresponding ECF at off-axis distances 9, 12, 15 and 18 arcmin. The parameters are given only for 10, 50, 75 and 90% ECF. The list of parameters for the full range 5-95% ECF is only available in online version of the paper.

ECF (%)	ART-XC mirror module															
	ARTM1		ARTM2		ARTM3		ARTM4		ARTM5		ARTM6		ARTM7		ARTM8	
	a (")	b (")	a (")	b (")	a (")	b (")	a (")	b (")	a (")	b (")	a (")	b (")	a (")	b (")	a (")	b (")
Off-axis 9 arcmin																
10	5.3	5.1	5.0	4.6	5.4	5.2	5.0	4.6	5.0	4.7	7.2	6.7	4.9	4.6	5.1	4.8
50	20.4	14.2	22.1	14.9	20.6	14.7	23.0	15.0	24.6	16.2	31.1	21.1	23.4	14.7	24.1	15.9
75	52.7	50.4	57.5	54.5	57.1	55.5	63.9	58.7	75.8	64.3	98.2	89.6	62.3	57.3	63.5	60.1
90	292.8	280.4	319.5	302.9	349.1	339.4	355.4	326.3	383.3	325.1	410.2	374.2	315.1	289.4	321.2	303.6
Off-axis 12 arcmin																
10	7.0	6.2	6.9	6.2	7.3	6.6	6.8	5.9	7.0	5.8	8.7	8.1	6.5	5.4	7.0	5.9
50	36.9	20.1	39.6	21.1	37.1	20.4	40.2	21.8	44.0	23.4	48.6	27.1	40.9	21.0	41.5	22.5
75	118.9	109.9	131.4	108.4	143.6	126.1	153.8	130.0	164.8	132.9	210.7	165.0	140.1	106.9	143.5	117.7
90	410.5	379.3	453.6	374.2	450.8	395.8	482.6	408.0	470.3	379.0	546.4	428.0	483.7	369.1	495.3	406.4
Off-axis 15 arcmin																
10	11.2	8.4	11.1	8.2	11.4	8.9	11.0	8.0	11.0	7.4	11.6	10.1	10.0	6.8	10.1	7.5
50	63.7	33.1	65.8	34.4	64.6	34.2	66.5	34.8	71.2	36.6	79.5	46.7	67.7	33.8	68.2	35.2
75	223.9	160.1	232.7	166.7	233.9	183.6	241.0	180.6	255.6	181.4	327.5	224.4	243.7	161.9	248.5	178.6
90	580.6	415.2	603.5	432.5	551.6	433.0	568.3	425.8	602.6	427.7	638.2	437.3	632.0	420.1	585.9	421.1
Off-axis 18 arcmin																
10	17.6	10.5	17.4	9.7	18.1	11.3	17.9	10.0	18.1	9.4	17.3	11.6	16.3	8.7	15.9	9.6
50	89.3	46.0	91.1	47.3	91.3	48.4	92.5	49.2	98.0	49.4	107.8	61.1	94.3	45.7	93.7	47.8
75	274.0	175.1	281.4	180.3	285.8	193.5	287.3	191.8	304.3	191.0	356.2	222.8	265.7	158.3	292.9	187.0
90	587.3	375.3	603.3	386.6	612.6	414.8	615.9	411.2	652.3	409.5	694.1	434.3	626.5	373.2	627.8	400.7

Table 5 Parameterization of the PSF for ARTM7 mirror module in a form of ellipse semi- major (a) and minor (b) axes with a corresponding ECF at angular distances 20', 22', and 24'.

ECF (%)	Off-axis distance (arcmin)					
	20		22		24	
	a (")	b (")	a (")	b (")	a (")	b (")
5	11.3	7.4	14.0	8.6	16.8	9.4
10	22.1	9.7	28.8	11.3	36.1	12.8
15	34.2	12.4	43.7	15.0	52.9	17.7
20	45.7	16.6	57.5	20.2	68.2	24.7
25	56.4	22.1	69.8	27.2	81.9	33.2
30	66.7	28.3	81.3	34.2	95.0	41.6
35	76.9	34.9	92.9	41.4	107.4	49.7
40	87.8	41.3	105.0	48.0	120.7	56.6
45	99.1	47.4	117.8	54.4	135.0	62.7
50	112.1	54.7	132.6	62.0	150.8	69.2
55	127.4	65.0	149.7	71.8	169.0	77.9
60	144.7	77.7	181.2	86.8	204.5	94.3
65	175.0	94.1	199.3	95.5	224.9	103.7
70	211.8	113.8	265.2	127.1	272.2	125.5
75	281.9	151.5	320.9	153.8	329.3	151.9
80	375.2	201.6	427.2	204.8	438.3	202.1
85	499.4	268.3	568.6	272.5	583.4	269.0
90	664.7	357.2	756.8	362.7	776.5	358.1
95	884.7	475.4	915.7	438.9	939.6	433.3

6 Summary and Future Work

We have analyzed PSF images acquired with a high-resolution CCD camera at different off-axis angles to build an analytical representation of the near on-axis ART-XC PSF by using a linear combination of King profiles to describe the core and broad wing of the PSF. We demonstrated that all seven X-ray optical modules have almost identical angular response, with HPD \sim 30 arcmin, and the deviations between the modules are within 10%. The ground testing routines with the X-ray beam facility at MSFC thus confirm the high angular performance of the ART-XC optics. The constrained parameter space enables, through interpolation between the reference points, modeling the PSF shape at any off-axis distances within 9 arcmin and for each individual ART-XC mirror module.

The ART-XC PSF at large off-axis distances, characterized by a strong elongation and shape distortions, was parameterized as a set of elliptical regions describing the enclosed count fraction (ECF). This approach allows us to characterize the complex morphology of the PSF in a simple way, which can be used later on in data reduction.

The constructed PSF model will be compared to testing results obtained at the X-ray beam facility at the Space Research Institute (IKI) in Moscow, where the spare ART-XC mirror module (ARTM6) is being extensively tested. Although the spare mirror module has the poorest imaging performance, its characteristics can be readily rescaled for every flight mirror system using the calibrated parameter space presented here.

The angular response of the optics was measured at MSFC at an almost monochromatic X-ray beam of a copper anode at energy ~ 8 keV. The ongoing testing routines at IKI are performed with the spare CdTe DSS detector, which can detect photons up to ~ 150 keV, well above the useful energy range of the ART-XC mirror modules. This allows us to investigate the energy dependence of the angular response and effective area of the ART-XC optics. The results of the calibration procedures at IKI will be presented elsewhere.

Acknowledgements The authors acknowledge support from the Russian Basic Research Foundation (grant 16-29-13070).

Appendix: online data

The following Tables A1-A4 correspond to Table 4 from the main paper “The calibration of ART-XC mirror modules at MSFC” and contain the extended parameterization of the ART-XC PSF in a form of ellipse semi-major (a) and minor (b) axes with a corresponding ECF at off-axis distances 9, 12, 15 and 18 arcmin. The parameters are given for the full range 5-95% ECF.

Table A1 Parameterization of ART-XC PSF in a form of ellipse semi-major (a) and minor (b) axes with a corresponding ECF at angular distance 9’.

ECF (%)	ART-XC mirror module															
	ARTM1		ARTM2		ARTM3		ARTM4		ARTM5		ARTM6		ARTM7		ARTM8	
	a (")	b (")	a (")	b (")	a (")	b (")	a (")	b (")	a (")	b (")	a (")	b (")	a (")	b (")	a (")	b (")
5	2.9	2.8	2.9	2.6	4.1	3.9	3.1	2.8	2.9	2.7	4.9	4.7	2.9	2.6	3.6	3.3
10	5.3	5.1	5.0	4.6	5.4	5.2	5.0	4.6	5.0	4.7	7.2	6.7	4.9	4.6	5.1	4.8
15	6.6	6.2	6.7	5.9	7.0	6.5	6.6	5.8	6.9	5.9	9.6	8.6	6.7	5.8	7.2	6.2
20	8.0	7.2	8.4	7.0	8.8	7.8	8.5	6.9	8.7	6.8	11.5	10.1	8.4	6.9	9.0	7.5
25	9.6	8.2	10.1	8.1	10.1	8.8	10.2	7.9	10.8	8.2	13.7	11.5	10.6	8.0	11.0	8.7
30	11.3	9.2	11.9	9.2	11.7	9.9	12.2	9.1	12.9	9.3	16.3	12.8	12.7	9.0	13.2	9.9
35	13.1	10.2	14.1	10.4	13.5	11.0	14.5	10.3	15.2	10.6	19.2	14.3	14.9	10.0	15.5	11.1
40	15.2	11.3	16.4	11.6	15.7	12.2	16.9	11.4	17.7	11.9	22.4	16.0	17.5	11.3	18.0	12.4
45	17.7	12.7	19.2	13.2	18.1	13.4	19.9	13.2	21.0	13.9	26.2	18.0	20.4	13.0	21.0	14.1
50	20.4	14.2	22.1	14.9	20.6	14.7	23.0	15.0	24.6	16.2	31.1	21.1	23.4	14.7	24.1	15.9
55	24.0	16.4	26.4	17.6	24.2	16.8	27.6	18.3	29.6	19.5	36.6	24.8	27.8	18.0	28.7	19.2
60	27.9	18.9	30.8	20.5	28.4	19.5	32.3	21.6	34.5	22.9	44.8	33.4	32.3	21.3	33.3	22.6
65	33.4	24.4	38.2	29.0	35.4	27.0	41.6	32.1	45.5	35.2	55.9	47.3	40.7	30.7	42.2	33.1
70	43.0	37.4	47.8	41.7	46.2	41.3	52.8	45.4	57.0	48.3	67.1	61.2	51.5	44.0	52.9	46.6
75	52.7	50.4	57.5	54.5	57.1	55.5	63.9	58.7	75.8	64.3	98.2	89.6	62.3	57.3	63.5	60.1
80	77.1	73.8	92.5	87.7	101.1	98.3	102.9	94.5	134.4	114.0	174.0	158.7	100.4	92.2	102.3	96.7
85	165.3	158.3	180.3	171.0	197.0	191.6	200.6	184.2	238.0	201.9	280.2	255.6	177.9	163.4	181.3	171.4
90	292.8	280.4	319.5	302.9	349.1	339.4	355.4	326.3	383.3	325.1	410.2	374.2	315.1	289.4	321.2	303.6
95	518.8	496.7	514.5	487.8	511.1	496.9	520.3	477.8	561.2	476.0	546.0	498.0	507.5	466.2	517.2	488.9

Table A2 Paramerization of ART-XC PSF in a form of ellipse semi- major (a) and minor (b) axes with a corresponding ECF at angular distance 12'.

ECF (%)	ART-XC mirror module															
	ARTM1		ARTM2		ARTM3		ARTM4		ARTM5		ARTM6		ARTM7		ARTM8	
	a (")	b (")	a (")	b (")	a (")	b (")	a (")	b (")	a (")	b (")	a (")	b (")	a (")	b (")	a (")	b (")
5	4.6	4.4	4.6	4.3	4.8	4.5	4.4	4.0	4.5	4.0	5.9	5.6	4.4	3.8	4.6	4.0
10	7.0	6.2	6.9	6.2	7.3	6.6	6.8	5.9	7.0	5.8	8.7	8.1	6.5	5.4	7.0	5.9
15	9.2	7.7	9.4	7.8	9.7	8.4	9.2	7.1	10.2	7.2	11.7	10.3	9.4	6.8	9.9	7.5
20	12.0	9.1	12.4	8.9	12.0	9.6	12.2	8.2	13.2	8.6	14.7	11.7	12.4	7.8	12.8	8.7
25	15.0	10.3	15.5	10.0	15.0	10.9	15.4	9.5	17.0	9.9	18.3	13.1	15.5	8.8	16.2	9.8
30	18.2	11.4	19.0	11.1	18.2	12.1	19.2	10.9	21.0	11.5	22.6	14.3	19.4	10.1	20.0	11.2
35	22.0	12.8	23.1	12.7	21.9	13.4	23.3	12.5	25.6	13.4	27.3	16.0	23.6	11.9	24.2	12.9
40	26.1	14.6	27.9	14.8	26.1	15.0	28.1	14.6	30.8	15.8	33.2	18.6	28.3	14.2	28.9	15.2
45	31.1	16.8	33.1	17.3	30.9	17.0	33.3	17.2	36.7	18.7	40.3	22.2	33.9	16.9	34.3	17.8
50	36.9	20.1	39.6	21.1	37.1	20.4	40.2	21.8	44.0	23.4	48.6	27.1	40.9	21.0	41.5	22.5
55	43.4	23.9	46.5	25.1	43.7	24.3	47.1	26.5	51.8	28.9	60.3	40.0	48.1	25.4	48.8	27.3
60	52.7	36.0	56.6	39.4	55.1	40.8	59.4	43.6	64.3	45.4	73.8	57.8	59.5	39.1	61.2	43.9
65	63.3	52.1	67.4	55.6	67.0	58.8	71.7	60.7	76.9	62.0	98.3	77.0	71.9	54.9	73.6	60.4
70	73.8	68.2	89.7	74.0	89.2	78.3	95.5	80.7	102.3	82.5	143.9	112.7	95.7	73.0	98.0	80.4
75	118.9	109.9	131.4	108.4	143.6	126.1	153.8	130.0	164.8	132.9	210.7	165.0	140.1	106.9	143.5	117.7
80	191.5	176.9	211.6	174.6	231.3	203.1	225.2	190.4	241.3	194.5	308.4	241.6	225.6	172.2	231.1	189.6
85	280.4	259.1	309.8	255.6	338.7	297.4	329.7	278.7	353.3	284.8	410.5	321.5	330.3	252.1	338.3	277.6
90	410.5	379.3	453.6	374.2	450.8	395.8	482.6	408.0	470.3	379.0	546.4	428.0	483.7	369.1	495.3	406.4
95	546.4	504.8	603.7	498.1	600.0	526.8	642.4	543.1	625.9	504.5	661.2	517.8	643.8	491.3	659.3	540.9

Table A3 Paramerization of ART-XC PSF in a form of ellipse semi- major (a) and minor (b) axes with a corresponding ECF at angular distance 15'.

ECF (%)	ART-XC mirror module															
	ARTM1		ARTM2		ARTM3		ARTM4		ARTM5		ARTM6		ARTM7		ARTM8	
	a (")	b (")	a (")	b (")	a (")	b (")	a (")	b (")	a (")	b (")	a (")	b (")	a (")	b (")	a (")	b (")
5	6.8	6.0	6.4	5.7	6.8	6.2	6.5	5.6	5.9	5.1	7.2	7.0	5.6	4.8	6.2	5.4
10	11.2	8.4	11.1	8.2	11.4	8.9	11.0	8.0	11.0	7.4	11.6	10.1	10.0	6.8	10.1	7.5
15	15.9	10.2	16.1	9.8	16.0	11.0	16.0	9.5	16.6	9.4	16.8	11.8	15.1	8.0	15.1	9.2
20	21.7	11.8	21.8	11.3	21.8	12.4	22.1	11.0	23.1	11.1	22.8	13.5	20.9	9.6	20.9	10.9
25	27.5	13.8	28.0	13.4	27.7	14.2	28.2	13.2	30.1	13.7	30.1	15.6	27.5	11.7	27.0	12.8
30	33.7	16.3	34.4	16.1	34.0	16.4	34.8	15.9	37.2	16.8	37.6	18.6	34.1	14.6	33.9	15.5
35	40.1	19.2	41.3	19.5	40.5	19.4	41.5	19.2	44.6	20.4	45.9	22.4	41.6	18.1	41.1	19.0
40	47.2	23.0	48.6	23.6	47.6	23.1	48.7	23.2	52.6	24.8	55.0	27.2	49.3	22.4	49.2	23.3
45	55.0	27.5	56.7	28.6	55.7	28.2	57.2	28.5	61.6	30.3	66.2	34.0	57.9	27.5	58.4	28.9
50	63.7	33.1	65.8	34.4	64.6	34.2	66.5	34.8	71.2	36.6	79.5	46.7	67.7	33.8	68.2	35.2
55	74.3	45.0	77.2	47.6	77.1	51.7	79.5	51.5	84.5	52.5	94.9	65.0	80.1	46.3	81.8	51.5
60	86.3	61.7	89.7	64.3	90.2	70.8	92.9	69.6	98.5	69.9	126.3	86.5	93.9	62.4	95.8	68.9
65	104.4	74.7	108.5	77.8	120.1	94.2	123.7	92.7	131.1	93.1	168.0	115.2	113.7	75.6	127.5	91.6
70	152.9	109.3	158.9	113.9	175.8	138.0	181.1	135.7	174.6	123.9	246.0	168.6	166.4	110.6	169.7	122.0
75	223.9	160.1	232.7	166.7	233.9	183.6	241.0	180.6	255.6	181.4	327.5	224.4	243.7	161.9	248.5	178.6
80	327.7	234.4	340.6	244.1	342.5	268.8	352.9	264.4	340.2	241.4	435.9	298.7	356.7	237.1	330.7	237.7
85	436.2	312.0	453.4	324.9	455.9	357.8	469.7	351.9	452.7	321.3	527.4	361.4	474.8	315.6	440.2	316.4
90	580.6	415.2	603.5	432.5	551.6	433.0	568.3	425.8	602.6	427.7	638.2	437.3	632.0	420.1	585.9	421.1
95	772.8	552.7	730.2	523.3	667.5	523.9	756.4	566.7	729.1	517.5	772.2	529.1	764.7	508.3	708.9	509.6

Table A4 Paramerization of ART-XC PSF in a form of ellipse semi- major (a) and minor (b) axes with a corresponding ECF at angular distance 18°.

ECF (%)	ART-XC mirror module															
	ARTM1		ARTM2		ARTM3		ARTM4		ARTM5		ARTM6		ARTM7		ARTM8	
	a (")	b (")	a (")	b (")	a (")	b (")	a (")	b (")	a (")	b (")	a (")	b (")	a (")	b (")	a (")	b (")
5	9.5	7.9	9.4	7.6	10.2	8.4	9.5	7.5	9.7	7.0	9.6	8.5	8.4	6.8	8.9	7.0
10	17.6	10.5	17.4	9.7	18.1	11.3	17.9	10.0	18.1	9.4	17.3	11.6	16.3	8.7	15.9	9.6
15	25.7	12.9	26.3	12.1	27.2	13.7	27.0	12.4	27.2	11.8	26.3	14.0	25.1	10.5	24.6	11.4
20	34.5	15.8	35.1	15.1	36.0	16.5	35.9	15.5	36.9	15.2	36.1	17.0	34.8	13.6	33.7	14.1
25	42.7	19.3	43.6	18.8	44.2	20.2	44.4	19.4	46.2	19.6	46.0	21.0	44.1	17.4	42.7	17.8
30	50.9	23.4	52.1	23.4	52.7	24.4	53.0	24.4	55.3	24.3	56.2	26.2	53.3	22.1	51.6	22.5
35	59.4	28.3	60.6	28.6	61.0	29.1	61.4	29.5	64.7	29.5	67.0	32.2	62.2	27.3	60.7	27.8
40	68.5	33.6	69.7	34.2	69.9	34.3	70.7	35.2	74.8	35.3	78.6	38.9	71.8	32.8	70.6	33.7
45	78.3	39.5	79.8	40.4	80.0	40.6	81.2	41.9	86.0	42.0	91.9	46.8	82.4	38.8	81.7	40.4
50	89.3	46.0	91.1	47.3	91.3	48.4	92.5	49.2	98.0	49.4	107.8	61.1	94.3	45.7	93.7	47.8
55	102.2	58.5	104.8	60.8	106.1	64.9	107.1	65.1	113.5	65.1	124.8	78.1	108.5	58.1	108.9	63.5
60	116.2	74.3	119.4	76.5	121.2	82.1	121.9	81.3	129.1	81.0	166.2	104.0	123.9	73.8	124.2	79.3
65	140.6	89.8	144.4	92.5	161.3	109.2	162.2	108.3	171.8	107.8	201.1	125.8	150.0	89.3	165.3	105.5
70	187.1	119.6	192.2	123.2	214.7	145.4	215.9	144.1	228.6	143.5	267.6	167.4	199.6	118.9	200.0	127.7
75	274.0	175.1	281.4	180.3	285.8	193.5	287.3	191.8	304.3	191.0	356.2	222.8	265.7	158.3	292.9	187.0
80	364.6	233.0	374.6	240.0	380.4	257.6	382.5	255.3	405.0	254.3	474.1	296.6	353.6	210.6	389.8	248.8
85	441.2	282.0	453.3	290.4	460.2	311.7	462.8	308.9	490.1	307.7	573.7	358.9	470.7	280.4	471.7	301.1
90	587.3	375.3	603.3	386.6	612.6	414.8	615.9	411.2	652.3	409.5	694.1	434.3	626.5	373.2	627.8	400.7
95	781.6	499.5	730.0	467.8	741.2	501.9	745.3	497.5	789.3	495.5	763.6	477.7	758.0	451.5	759.6	484.9

References

1. P. Predehl, R. Andritschke, V. Babyshkin, W. Becker, W. Bornemann, H. Bräuninger, H. Brunner, T. Boller, V. Burwitz, W. Burkert, N. Clerc, E. Churazov, D. Coutinho, K. Dennerl, T. Dwelly, J. Eder, V. Emberger, M. Freyberg, P. Friedrich, M. Fürmetz, A. Georgakakis, M. Gilfanov, C. Grossberger, F. Haberl, O. Hälker, G. Hartner, A.V. Kienlin, W. Kink, I. Kreykenbohm, G. Lamer, I. Lomakin, I. Lapshov, N. Meidinger, A. Merloni, B. Mican, S. Müller, K. Nandra, M. Pavlinsky, E. Pfeffermann, D. Pietschner, J. Robrade, M. Salvato, A. Santangelo, M. Sasaki, H. Scheuerle, J. Schmitt, A. Schwobe, R. Sunyaev, C. Tenzer, V. Yaroshenko, J. Wilms, in *Space Telescopes and Instrumentation 2016: Ultraviolet to Gamma Ray*, *Proc. SPIE*, vol. 9905 (2016), *Proc. SPIE*, vol. 9905, p. 99051K. DOI 10.1117/12.2235092
2. M. Pavlinsky, V. Akimov, V. Levin, A. Krivchenko, A. Rotin, M. Kuznetsova, I. Lapshov, A. Tkachenko, N. Semena, M. Buntov, A. Glushenko, V. Arefiev, A. Yaskovich, S. Grebenev, S. Sazonov, M. Revnitsev, A. Lutovinov, S. Molkov, R. Krivonos, D. Serbinov, M. Kudelin, T. Drozdova, S. Voronkov, R. Sunyaev, E. Churazov, M. Gilfanov, V. Babyshkin, I. Lomakin, A. Menderov, M. Gubarev, B. Ramsey, K. Kilaru, S.L. O'Dell, J. Kolodziejczak, R. Elsner, V. Zavlin, D. Swartz, in *Space Telescopes and Instrumentation 2016: Ultraviolet to Gamma Ray*, *Proc. SPIE*, vol. 9905 (2016), *Proc. SPIE*, vol. 9905, p. 99051J. DOI 10.1117/12.2230974
3. M. Gubarev, B. Ramsey, S.L. O'Dell, R. Elsner, K. Kilaru, J. McCracken, M. Pavlinsky, A. Tkachenko, I. Lapshov, in *Space Telescopes and Instrumentation 2012: Ultraviolet to Gamma Ray*, *Proc. SPIE*, vol. 8443 (2012), *Proc. SPIE*, vol. 8443, p. 84431U. DOI 10.1117/12.926207
4. M. Gubarev, B. Ramsey, S.L. O'Dell, R. Elsner, K. Kilaru, J. McCracken, M. Pavlinsky, A. Tkachenko, I. Lapshov, C. Atkins, V. Zavlin, in *Optics for EUV, X-Ray, and Gamma-Ray Astronomy VI*, *Proc. SPIE*, vol. 8861 (2013), *Proc. SPIE*, vol. 8861, p. 88610K. DOI 10.1117/12.2027141
5. M. Gubarev, B. Ramsey, R. Elsner, S. O'Dell, J. Kolodziejczak, J. McCracken, V. Zavlin, D. Swartz, K. Kilaru, C. Atkins, M. Pavlinsky, A. Tkachenko, I. Lapshov, in *Space Telescopes and Instrumentation 2014: Ultraviolet to Gamma Ray*, *Proc. SPIE*, vol. 9144 (2014), *Proc. SPIE*, vol. 9144, p. 91441V. DOI 10.1117/12.2056813

6. B.D. Ramsey, R.F. Elsner, D.E. Engelhaupt, S.L. O'Dell, C.O. Speegle, M.C. Weisskopf, in X-Ray and Gamma-Ray Telescopes and Instruments for Astronomy, Proc. SPIE, vol. 4851, ed. by J.E. Truemper, H.D. Tananbaum (2003), Proc. SPIE, vol. 4851, pp. 631–638. DOI 10.1117/12.461597
7. B.D. Ramsey, Experimental Astronomy **20**, 85 (2005). DOI 10.1007/s10686-006-9033-6
8. K.K. Madsen, F.A. Harrison, C.B. Markwardt, H. An, B.W. Grefenstette, M. Bachetti, H. Miyasaka, T. Kitaguchi, V. Bhalerao, S. Boggs, F.E. Christensen, W.W. Craig, K. Forster, F. Fuerst, C.J. Hailey, M. Perri, S. Puccetti, V. Rana, D. Stern, D.J. Walton, N. Jørgen Westergaard, W.W. Zhang, ApJS**220**, 8 (2015). DOI 10.1088/0067-0049/220/1/8
9. I. King, AJ**67**, 471 (1962). DOI 10.1086/108756
10. C. Allen, D.H. Jerius, T.J. Gaetz, in X-Ray and Gamma-Ray Instrumentation for Astronomy XIII, Proc. SPIE, vol. 5165, ed. by K.A. Flanagan, O.H.W. Siegmund (2004), Proc. SPIE, vol. 5165, pp. 423–432. DOI 10.1117/12.509411